Under the Influence of Alcohol: The Effect of Ethanol and Methanol on Lipid Bilayers

Michael Patra,*[†] Emppu Salonen,[‡] Emma Terama,[‡] Ilpo Vattulainen,[‡] Roland Faller,[§] Bryan W. Lee,[§] Juha Holopainen,[¶] and Mikko Karttunen*

*Biophysics and Statistical Mechanics Group, Laboratory of Computational Engineering, Helsinki University of Technology, Helsinki, Finland; [†]Physical Chemistry 1, Centre for Chemistry and Chemical Engineering, Lund University, Lund, Sweden; [‡]Laboratory of Physics and Helsinki Institute of Physics, Helsinki University of Technology, Helsinki, Finland; [§]Department of Chemical Engineering and Materials Science, University of California-Davis, Davis, California; [¶]Department of Ophthalmology, and Helsinki Biophysics & Biomembrane Group, Institute of Biomedicine, University of Helsinki, Helsinki, Finland; and Department of Applied Mathematics, University of Western Ontario, London, Ontario, Canada

ABSTRACT   Extensive microscopic molecular dynamics simulations have been performed to study the effects of short-chain alcohols, methanol and ethanol, on two different fully hydrated lipid bilayer systems (POPC and DPPC) in the fluid phase at 323 K. It is found that ethanol has a stronger effect on the structural properties of the membranes. In particular, the bilayers become more fluid and permeable: ethanol molecules are able to penetrate through the membrane in typical timescales of ~200 ns, whereas for methanol that timescale is considerably longer, at least of the order of microseconds. A closer examination exposes a number of effects due to ethanol. Hydrogen-bonding analysis reveals that a large fraction of ethanols is involved in hydrogen bonds with lipids. This in turn is intimately coupled to the ordering of hydrocarbon chains: we find that binding to an ethanol decreases the order of the chains. We have also determined the dependence of lipid-chain ordering on ethanol concentration and found that to be nonmonotonous. Overall, we find good agreement with NMR and micropipette studies.

INTRODUCTION

It is well known that even small changes in the composition of cell membranes can strongly affect the functioning of intrinsic membrane proteins, such as ion and water channels, which regulate the chemical and physical balance in cells (1,2). Such changes may occur due to the introduction of short-chain alcohols, or other anesthetics, at membrane surfaces. Although anesthetics are being used every single day in hospitals around the world, the molecular level mechanisms of general anesthesia remain elusive (see e.g., (3–5)). The same applies to the effect of alcohols on biological systems. Klemm (6) provides a good review of the topic.

Another aspect to the effect of alcohols appears in a more applied context. In the process of producing alcoholic beverages, wine in particular, yeasts like *Saccharomyces cerevisiae* have to sustain high ethanol concentrations without losing their viability. However, in ~10% of all wine fermentations, the industry encounters so-called stuck fermentations (7,8). There is no satisfactory understanding of this effect. Some models propose that an effect very similar to general anesthesia is responsible for rendering the yeast cells dormant (9). It has been suggested that high alcohol concentrations change the membrane structure and force transmembrane proteins into unfavorable conformations. In these conformations, proteins cannot fulfill their functions and thus the yield drops dramatically.

In addition to the above aspects, there are also other important issues. In particular, in cellular systems such as bacteria and yeast, the toxicity of ethanol has been suggested to

be due to its interaction with membranes (8,10,11) and the consequent general effects such as changes in the mechanical properties of permeability and diffusion. Changes in such generic membrane properties may affect the functions of proteins and binding sites due to changes in lateral pressure (4), or, if the membrane becomes more permeable, changes in the electrostatic potential may affect signaling. These effects are not to be mixed up with the toxicity due to metabolic products such as acetaldehyde from consumption of ethanol—the cause of poisoning commonly known as hangover.

We concentrate on the effects of ethanol and methanol on structural properties of membranes. It is quite surprising that despite a vast number of clinical and biochemical studies, there have been very few computational investigations of the effect of short-chain alcohols, or other anesthetics, on membranes. The only simulational studies of bilayers and ethanol are, to the authors' knowledge, the one by Feller et al. (12), who used molecular dynamics simulations of ethanol and palmitoyloleoylphosphatidylcholine (POPC) lipid bilayers and NMR to study the molecular level interactions in these systems, and the article by Lee et al. (13) discussing alcohol-membrane systems briefly. Direct comparison of all of our results with Feller et al. (12) is not meaningful since their study was performed using a different ensemble, alcohol concentration, and with different hydration. For methanol-bilayer systems there exists, to the authors' knowledge, only one computational article (14).

For anesthetics, the situation is slightly better. Tang and Xu (5) used molecular dynamics simulations to study molecular level mechanisms of general anesthesia using halothane as a specific anesthetic. They concluded that the global effects

of anesthetics, i.e., due to generic interaction mechanisms, are important and lead to modulations in the functions of channels and/or proteins. These conclusions are also supported by the fact that the same anesthetics are effective for humans and a variety of animals. Similar conclusions for halothane interactions with bilayers have been pointed out by Koubi et al. (15,16). The importance of generic effects has also been indicated in recent experimental studies of the effect of ethanol on *Oenococcus oeni* cells (8). Although the shortage of simulational studies may be due to the high computational demands of these systems, it is still surprising since computer simulations can provide detailed information about fundamental molecular level mechanisms.

In this article, we study the effect of two short-chain alcohols, ethanol and methanol, on two different lipid membranes consisting of either pure dipalmitoylphosphatidylcholine (DPPC) or POPC. Methanol is a small solute having a single hydrophilic hydroxyl group whereas ethanol possesses an additional hydrophobic carboxyl group. DPPC and POPC share the same headgroup but one of the chains of POPC has a double bond and is two carbon-atoms longer, whereas DPPC has only single bonds in its chains (see Fig. 1). We have studied these systems under fully hydrated conditions using atomistic molecular dynamics. Fifty-nanosecond trajectories for each of the four combinations of lipid and alcohol allow us to gather high statistical accuracy.

Phospholipid bilayers can be considered as a first approximation to understand the behavior of cell membranes under the influence of alcohol, and much information can be extracted from such systems. Our simulations show that ethanol is able to pass through the bilayer much more easily than methanol. This can be explained by the hydrophobic nature of the carbon tail of ethanol, making passing through the hydrophobic chain regions of lipid bilayers easier. In addition, ethanol molecules condense near the interface region between lipids and the surrounding water, i.e., there is a sharply increased density of ethanol near the interface region, whereas for
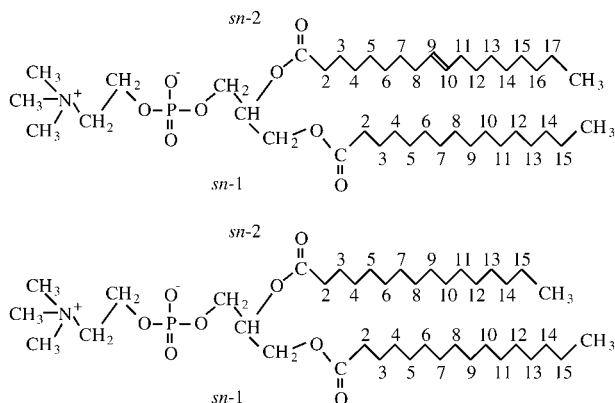

FIGURE 1 Structures of POPC (*top*) and DPPC (*bottom*). They are identical with the exception of the *sn*−2 chain, which is two carbons longer and contains one double bond for POPC.

methanol, only a moderate increase of the density is seen near the region of the interface. These effects are very pronounced for DPPC bilayers, and only slightly weaker for POPC bilayers. This has far reaching implications for the basic properties of bilayers.

The rest of this article is organized as follows. In the next section, we describe the model and the simulation details. Then, in Simulation Results, we present the results from the simulations. Discussion contains a discussion and conclusions.

MODEL AND SIMULATION DETAILS

We have simulated lipid bilayer systems consisting of either 128 DPPC or 128 POPC molecules (i.e., 64 lipids in each leaflet). For the lipids, we used a previously validated united-atom model (17). The DPPC simulations are based on the final structure of a 100-ns run of a DPPC bilayer that is fully hydrated by 3655 water molecules. The configuration is available online (http://www.softsimu.org/downloads.shtml/). The simulations by Patra et al. (18) were run using the same parameters as here (details below), and the 100-ns run used in this study is a continuation of a 50-ns DPPC study (18,19). For the POPC simulations, such an initial structure had to be generated first. We started with a fully hydrated POPC bilayer (20) and simulated it for 10 ns. The final structure of that simulation run was used as a starting point for the POPC simulations reported here.

To add the alcohol molecules, the simulation box was first extended in the z direction such that an empty volume was created. A total of 90 ethanol (methanol) molecules were randomly inserted in the empty volume, and the remaining space was filled with water. The total number of water molecules then amounted to 8958 for the DPPC systems and 8948 for the POPC systems, or, in other words, 1 mol % alcohol on a lipid free basis. The small difference between DPPC and POPC systems is due to the different lateral extensions of the bilayers.

In addition to the above systems, we performed additional simulations in which the number of ethanol molecules was varied between 45 and 450 molecules. They were needed for a detailed comparison with experiments and other simulations (12,21). These results are briefly discussed in Order Parameters. A thorough report of these studies will be published later.

The force-field parameters for bonded and nonbonded interaction were taken from Berger et al. (22), available online (http://moose.bio.ucalgary.ca/downloads/files/lipid.itp). Partial charges were taken from Tieleman and Berendsen (17), available online for both DPPC and POPC (http://moose.bio.ucalgary.ca/downloads/files/dppc.itp and http://moose.bio.ucalgary.ca/downloads/files/popc.itp, respectively). As is seen in the chemical structures in Fig. 1, DPPC and POPC are identical up to a single pair of CH-groups, connected by a double bond instead of a single bond in the *sn*−2 chain of

POPC, and the two additional CH_2 groups at the end of that chain. This similarity is reflected in the force fields, which are identical up to the modeling of the four affected atoms. Ethanol and methanol were modeled using the GROMACS force-field parameters (23), which are identical with the exception of the added CH_2 group for ethanol. Thus, differences observed between the two lipids or the two alcohols do not originate from differences in their respective force-field parameterizations but are due to the physics and/or chemistry of those components. For water, the simple-point charge model (24) was used.

The simulations were performed with the GROMACS package (23). The lipids, water molecules, and alcohols were separately coupled to a heat bath at temperature $T = 323$ K using the Berendsen thermostat (25) with a coupling time-constant of 0.1 ps. All the bond lengths were constrained to their equilibrium values by the LINCS algorithm (26). Pressure was controlled using the Berendsen barostat (25) with a time constant of 1 ps. The pressure coupling was used semi-isotropically such that height of the box (z direction) and the cross-sectional area (x,y plane) were allowed to vary independently of each other. Lennard-Jones interactions were cut off at a distance of 1.0 nm and the time step was set to 2 fs. Long-range electrostatics were updated every 10th time step (the twin-range scheme (27,28) was used), and handled by the particle-mesh Ewald algorithm (29). For DPPC bilayers, it has been shown that replacing the particle-mesh Ewald by the computationally cheaper cutoff scheme leads to pronounced artifacts (18,28).

The systems were simulated for a total of 50 ns each. After 20 ns, the samples had equilibrated, and the remaining 30 ns were used for data collection. Equilibration was determined by monitoring the area per lipid as described in the next section. For completeness, we also present results for pure DPPC and POPC bilayers. In particular, the latter ones are important since many of the results published so far are based on simulations using a cutoff for handling electrostatics.

The simulations took ~16,000 CPU hours on an IBM eServer Cluster 1600 (Power4 processors).

SIMULATION RESULTS

Before presenting a systematic summary of our results, we give a quick overview of the basic properties of these systems. In a membrane, alcohol molecules have a tendency to collect in or near the bilayer-water interface region (see Mass Density, below). Ethanol is able to form hydrogen bonds with the lipids in the bilayer (see Hydrogen Bonding of Alcohol to Lipids, below), and these hydrogen bonds reduce the order parameter of the lipid hydrocarbon chains. The combination of these aspects results in an easy penetration of ethanol through the bilayer. In contrast, no hydrogen bonds or penetration was observed for methanol.

In this article, we use the following color code for all figures: Curves for systems containing ethanol are drawn in red; curves for methanol in green; and pure lipid systems without alcohol, in blue.

System dimensions

The area per lipid is one of the most important quantities characterizing lipid bilayer systems and it can also be used to monitor equilibration during a simulation run. The time evolutions of the area per lipid in the systems studied here are shown in Fig. 2. The average areas per lipid, $\langle A \rangle$, obtained in our simulations are listed in Table 1.

For a pure DPPC bilayer, we obtain $\langle A_{\mathrm{DPPC}} \rangle = 0.655$ nm^2, agreeing well with previous simulations and experiments (see (28) and references therein). For pure POPC, we obtain $\langle A_{\mathrm{POPC}} \rangle = 0.677$ nm^2, in agreement with previous computational studies (30,31) and slightly larger than the results from x-ray diffraction studies (32,33). For POPC, the difference to x-ray diffraction results, $\langle A_{\mathrm{POPC}} \rangle \approx 0.61$ nm^2, may be due to differences in *trans-gauche* conformational changes.

As seen from Table 1, the presence of alcohol has a small but nonvanishing effect on the area per lipid. The number of water molecules per lipid molecule plays only a minor role, as was verified by an additional simulation of DPPC with ethanol and a reduced amount of water. Interestingly, ethanol and methanol have almost the same effect on the area per lipid.

Although the definition of the area per lipid is straightforward, the same is not true for the volume occupied by a lipid. The precise definition of the volume V (or the thickness d) of a membrane is nontrivial, as discussed at length by Armen et al. (34). Here, we chose an operational definition based on local mass density. Other definitions, e.g., employing the electron density, are equally possible.

Below, we give the two definitions we used to compute the thickness. If ρ_{lipid}, ρ_{water}, and ρ_{alcohol} are the mass densities of the three components, the effective thickness of a single leaflet can be defined by

$$d_1 = \frac{1}{2} \int \frac{\rho_{\mathrm{lipid}}}{\rho_{\mathrm{lipid}} + \rho_{\mathrm{water}} + \rho_{\mathrm{alcohol}}} \, \mathrm{d}z, \tag{1a}$$

$$d_2 = \frac{1}{2} \int \frac{\rho_{\mathrm{lipid}}}{\rho_{\mathrm{lipid}} + \rho_{\mathrm{water}}} \, \mathrm{d}z. \tag{1b}$$
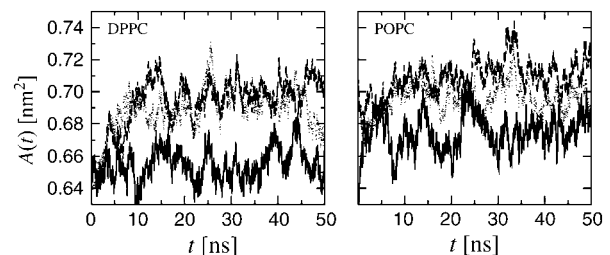

FIGURE 2 Temporal behavior of the area per lipid $A(t)$ for a DPPC bilayer (*left*) and a POPC bilayer (*right*). The color of the line marks whether the lipid bilayer has been simulated in the presence of ethanol (*dashed line*), methanol (*dotted*), or no alcohol (*solid*).

TABLE 1 **Average area per lipid for all systems studied in this work**

System	Average area per lipid
DPPC (pure)	(0.655 ± 0.002) nm^2
DPPC + ethanol	(0.699 ± 0.002) nm^2
DPPC + methanol	(0.693 ± 0.004) nm^2
POPC (pure)	(0.677 ± 0.003) nm^2
POPC + ethanol	(0.699 ± 0.003) nm^2
POPC + methanol	(0.693 ± 0.003) nm^2

A weak effect of the alcohols is visible. The error estimates have been computed from block averaging and extrapolating to large block sizes.

These two definitions differ in their treatment of the alcohol volume fraction and give the same thickness for pure lipid bilayers. After defining the thickness, the volume is simply $V = d\langle A \rangle$, with $\langle A \rangle$ being the average area per lipid. The results using both of the above definitions are summarized in Table 2.

The thicknesses we obtained for pure POPC agree very well with recent x-ray diffraction studies of Vogel et al. (35) and computer simulation studies of Gillingsrud and Schulten (36), who obtained 3.9 nm and 3.92 nm, respectively, for the total bilayer thickness $2\,d$. For DPPC, the thickness and volume are a few percent larger than the experimental results (37). Using the electron density to define the thickness would have led to similar results (see Electron Density, below).

A comparison of Tables 1 and 2 shows that the addition of ethanol or methanol to a bilayer expands its surface slightly, whereas the thickness decreases such that the volume per lipid does not change significantly. This is as expected, since the main effect of the addition of alcohol is a reduction of the surface tension of the water phase. This is in agreement with observations from a DPPC-halothane system (38). We will return to this issue in Discussion, below.

To complement the average area per lipid $\langle A \rangle$ measurements, we have also computed the area probability distribution $P(A)$ by Voronoi tessellation. By definition, Voronoi tessellation measures the area that is closer to a given molecule than to any other one. The Voronoi approach does not uniquely specify which point should be used to represent the entire molecule. We used the center-of-mass position of each lipid, projected onto the x,y plane. Other choices are also

possible, such as the position of the $sn-3$ carbon, which gives a better indication of the backbone of the lipid, whereas the center-of-mass describes the entire lipid.
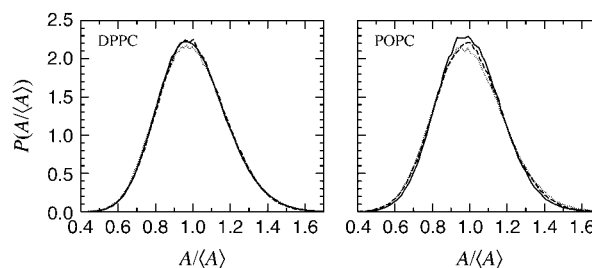
The resulting distributions $P(A)$ are shown in Fig. 3. The mean of that distribution is, by construction, identical to the average area per lipid as shown in Table 1, and thus does not contain any additional information. For this reason, not the plain distribution $P(A)$ but rather the rescaled distribution $P(A/\langle A \rangle)$ is shown in Fig. 3. Plotting the result in this way shows that alcohol does not influence the Voronoi distribution in any way that would not be captured already by the average area per lipid.

It is also possible to compute the autocorrelation time of the Voronoi areas. This time gives an indication of how quickly the geometry of the bilayer changes locally, whereas the fluctuations in the size of the simulation box seen in Fig. 2 are related to global changes of the geometry. The results are shown in Fig. 4. The faster decay for the systems with ethanol suggests that the bilayer might become more fluid, but care should be taken in drawing conclusions as the differences between the curves are rather small.

Next, we perform similar Voronoi tessellation for the alcohol molecules inside the bilayer interface region. The precise definition of that region turned out not to be critical, and we included all alcohol molecules within the range 0.7 nm $< z <$ 1.7 nm from the center of the bilayer. (Our choice for this range is motivated by the results to be discussed later in Mass Density, below.) The variable number of molecules forbids a proper calculation of the correlation time for the areas assigned to each alcohol, though, and thus we present only the distribution $P(A)$ in Fig. 5. Since there are fewer methanol molecules close to the bilayer than there are ethanols (see Fig. 6), the average area per methanol is larger than the average area per ethanol.

Mass density

The mass density profiles across the bilayer are shown in Fig. 6. For each analyzed simulation frame, the system was first translated such that the center of the bilayer was located at $z = 0$ to reduce statistical error. The masses of the hydrogen atoms were accounted for in the calculation. Due to the low

TABLE 2 **The thickness d of a leaflet (the bilayer thickness is twice that value) and the corresponding volume per lipid using the two definitions given in Eq. 1**

System	d_1 [nm]	V_1 [nm^3]	d_2 [nm]	V_2 [m^3]
DPPC (pure)	2.02 ± 0.05	1.32 ± 0.03	2.02 ± 0.05	1.32 ± 0.03
With ethanol	1.84 ± 0.02	1.28 ± 0.02	1.90 ± 0.02	1.33 ± 0.02
With methanol	1.93 ± 0.06	1.34 ± 0.04	1.95 ± 0.06	1.35 ± 0.04
POPC (pure)	1.96 ± 0.04	1.33 ± 0.03	1.96 ± 0.04	1.33 ± 0.03
With ethanol	1.87 ± 0.02	1.31 ± 0.02	1.93 ± 0.03	1.35 ± 0.02
With methanol	1.94 ± 0.02	1.35 ± 0.01	1.96 ± 0.02	1.36 ± 0.01

The error estimate for d has been computed by cutting the analysis part of the trajectory in two parts and by applying Eq. 1 separately to both of them.

FIGURE 3 Distribution of the individual areas of the lipids as determined by two-dimensional Voronoi tessellation for DPPC (*left*) and POPC (*right*).
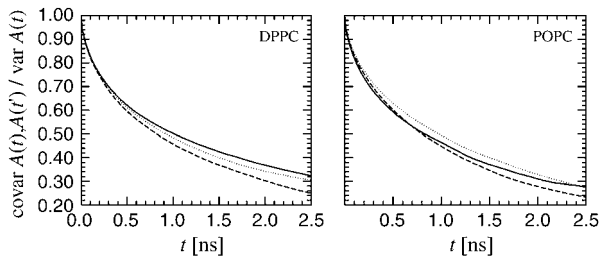
FIGURE 4 Autocorrelation function for the individual areas of the lipids as determined by two-dimensional Voronoi tessellation for DPPC (*left*) and POPC (*right*).

FIGURE 6 Mass density profiles across the bilayer for DPPC (*left*) and POPC (*right*). The density of the alcohol has been scaled by a factor of 10, and the color code is the same as above.

density of alcohol, its curve is scaled by a factor of 10 in the figure.

Additional information can be gained by considering separately the two charged groups in the lipid headgroups, namely the phosphate (P) and the choline (N) group (see Fig. 1). In addition to this, the oxygen atom of the alcohols is included in Fig. 7. We could not find a direct comparison for the mass density but the observations from the computer simulations of Feller et al. (12) are consistent with our results for the mass density. Fig. 7 shows that the alcohol molecules have a strong tendency to accumulate below the bilayer-water interface layer (approximately given by the location of the phosphate and choline groups), and that this tendency is stronger for ethanol than for methanol. (We will return to this issue; see Hydrogen Bonding of Alcohol to Lipids; Order Parameters; and Cross Events, below.)

The density of the lipid is decreased near the center of the bilayer. This phenomenon is known as a lipid trough, and means that the two leaflets are repelling each other. Still, the tails of the lipids from one leaflet are able to penetrate into the other leaflet; this is known as interdigitation (39). To analyze this, in Fig. 8 we plot the density throughout the whole bilayer, i.e., the positions of all atoms are not folded into a single leaflet. We show separately the density of the lipids belonging to the upper and the lower leaflet of the bilayer. It is easily seen that the tails of the lipids can penetrate up to 0.5 nm into the other leaflet, and the degree of

interdigitation is largely independent of the presence of alcohol.

Electron density

Electron densities provide information about the structure of bilayers along the normal to the bilayer plane similar to the mass densities. Experimentally, x-ray diffraction provides a means to access this quantity, the measurements yielding information of the total electron density profile.

Fig. 9 shows the total electron densities in different cases. For the pure lipid bilayers, the curves show the typical behavior, namely a maximum associated with the electron-dense areas in the headgroup, i.e., the phosphate groups, and the minimum at the bilayer center—the so-called methyl trough (37). Experimentally, an electron density profile contains different information, than a mass density profile since the chemical composition at depth z is not known directly. (For computer simulations, this problem does not exist.)

For the pure systems, our results agree well with experiments (40). The only x-ray diffraction study in a related system containing ethanol or methanol that we are aware of is that of Adachi (41). Unfortunately, a direct comparison is not meaningful, since that study was done in the gel phase using multilamellar vesicles, as compared to the fluidlike phase and planar bilayer system studied here.
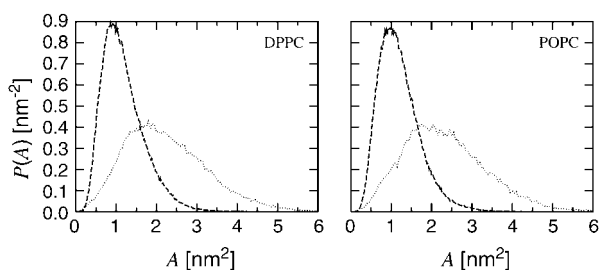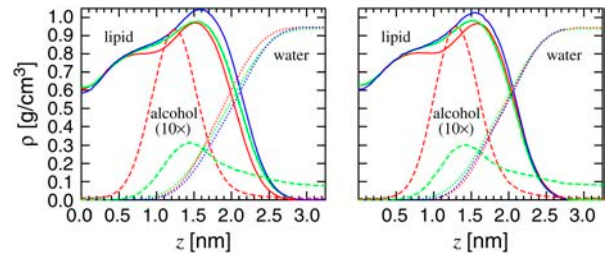

FIGURE 5 Distribution of the Voronoi areas of the alcohols with DPPC (*left*) and POPC (*right*). Only alcohol molecules located close to the bilayer interface are included in the analysis.
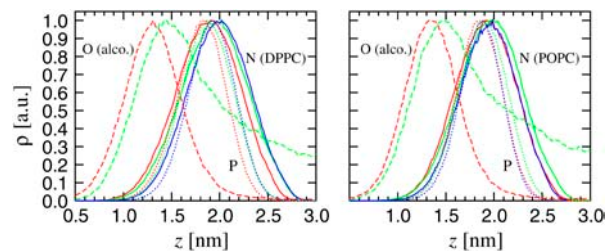

FIGURE 7 Mass density profiles across the bilayer. The densities given are the O(xygen) of alcohol as well as N(itrogen) and P(hosphorus) of the lipid, and scaled to give a maximum of unity. Left for DPPC, right for POPC.
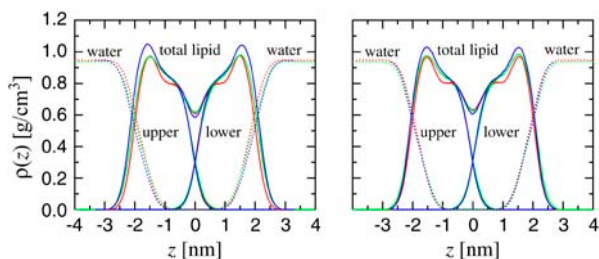
FIGURE 8 Density profile across the whole bilayer. The lipid component is divided into the contributions from the two separate leaflets, providing a measure of interdigitation. The alcohol component has been suppressed in the figure. Left for DPPC, right for POPC.

Hydrogen bonding of alcohol to lipids

As was shown in Electron Density, above, the alcohol molecules have a tendency to be located inside the bilayer, and this tendency is stronger for ethanol than for methanol. The alcohol molecules are not located directly at the water-membrane interface; instead, they are located further inside the bilayer. For the simulations with ethanol, a direct visual inspection of the atom positions shows that ethanol molecules are located close to the ester oxygens of the lipids (see Fig. 10).

This visual conclusion is confirmed by a hydrogen-bonding analysis. In such an analysis, possible donors and acceptors are identified by their chemical properties, and a hydrogen bond is then assumed to exist whenever two such atoms and an additional hydrogen atom fulfill certain geometric conditions. (The distance between a hydrogen and an acceptor has to be smaller than 0.25 nm, and the angle between acceptor, hydrogen, and donor has to be smaller than 60°.)

The hydrogen-bonding analysis shows that majority of the ethanols are involved in hydrogen bonds with lipids, whereas not a single hydrogen bond between a methanol and a lipid molecule was found in our simulations. The results are summarized in Table 3. Many lipids are involved in more than one hydrogen bond, which comes as no surprise since they possess an ester oxygen in each of their two chains. Comparison with the lifetime data for ethanol in Table 3 with NMR experiments of Holte and Gawrisch (42) shows
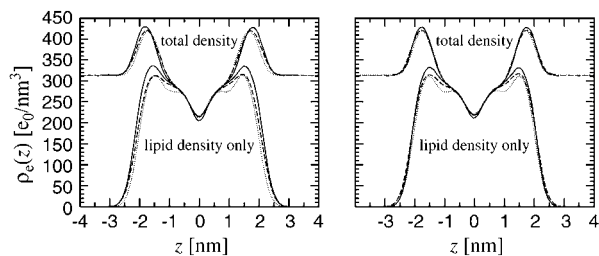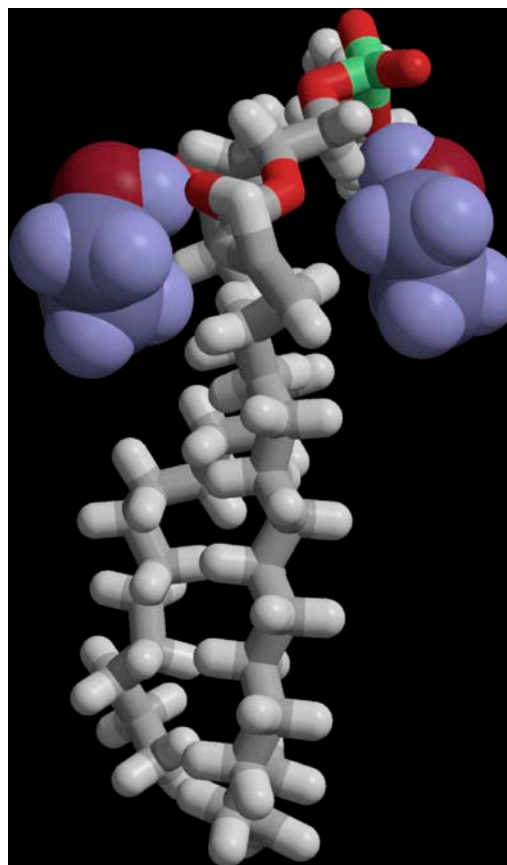

FIGURE 10 A DPPC molecule together with two ethanol molecules. The ethanols are located close to the ester oxygen. The DPPC molecule is drawn as rods, whereas the ethanols are drawn in a spacefilling representation. To aid the eye, the ethanols are colored blue.

excellent agreement. They reported the lifetimes to be ∼1 ns, whereas we obtained 1.20 ns for the ethanol lipid hydrogen bonds. We are not aware of any such experiments for methanol.

The number of alcohol molecules involved in hydrogen bonds is best compared against the total number of alcohol molecules located inside the bilayer. The latter number is relatively ill-defined but from Fig. 6 one can easily compute that for ethanol-containing systems only ∼10 ethanol molecules out of the ∼70 inside the bilayer are not involved in hydrogen bonds. For comparison, in the methanol systems

FIGURE 9 Electron density profiles in the studied systems with DPPC (left) and POPC (right).

TABLE 3 Results of the hydrogen bonding analysis for the DPPC and POPC bilayers with ethanol

	DPPC	POPC
Bound ethanols	72.9	71.6
Bound lipids	59.7	59.2
Hydrogen bonds	74.1	72.8
Lifetime [ns]	1.20	1.15

128 lipids and 90 alcohol molecules. No hydrogen bonds between methanol and lipids were found.

there are ~20 methanol molecules inside the bilayer and none of them is involved in hydrogen bonds (but see Cross Events, below). These numbers show that there is, indeed, a significant difference between ethanol and methanol.

Hydrogen-bonding analysis offers a well-defined criterion to decide whether a given lipid is interacting strongly with an alcohol molecule. This will be used in the later on to study separately the two lipid populations, lipids bound to an alcohol and lipids not bound to an alcohol.

Radial-distribution functions

In addition to the mass density profiles, valuable information may be gained from radial-distribution functions (RDFs), denoted as $g(r)$. They give the probability of finding two particles at a mutual distance r once geometric and density factors have been scaled out.

Fig. 11 shows the RDFs between the oxygen of the alcohol and different charged groups inside the lipid. Some of these groups were depicted already in the mass density profile in Fig. 7 but, because only the vertical distance between particles was considered, the RDF uses the real three-dimensional distance between them.

The mass density profile showed that, on the average, ethanol molecules prefer to reside 0.5 nm below the lipid headgroups, whereas the RDF shows that the three-dimensional preferred distance is only 0.38 nm. This is no contradiction but is easily understood by the observation (see Fig. 18 further down) that lipid molecules without an attached ethanol molecule are sticking out of the bilayer more than those with an attached ethanol. This is captured by the RDFs, but not by the mass density profile.

The radial-distribution functions for the different systems look quite similar, with one exception: the RDF between the alcohol and the ester group peaks at a much smaller distance for ethanol than for methanol. This is in agreement with the results of the hydrogen bonding analysis above.

By studying the mutual RDFs of the choline and/or phosphate groups, it is possible to detect phase transitions of the bilayer. Within error margins, these RDFs are not dependent

on the presence of alcohol, and for space reasons we do not show them here, because they are identical to the RDFs published previously (18).

We have also studied two-dimensional radial-distribution functions of entire molecules, i.e., the molecules' centers-of-mass were projected onto the x,y plane and radial-distribution functions were then computed. The results are shown in Fig. 12. The mutual radial-distribution functions of the lipids exhibit a very soft core, as lipids are able to wrap around each other. No dependence on lipid type or presence of alcohol was observed.

The RDF between alcohol and lipid is qualitatively different for ethanol and methanol. For an ethanol, there is a large probability for it to be at the same x,y position as the center-of-mass of the lipid. This reflects the hydrogen bonding of ethanol close to the center of the lipid. This bonding is absent for methanol, and consequently $g(r) \rightarrow 0$ for $r \rightarrow 0$. No significant dependence on the lipid type was observed.

The alcohol-alcohol radial-distribution functions have a very different character: for methanol with DPPC, the first peak is very distinct, but the correlations decay soon after. For methanol with POPC, an additional peak is observed. (This is the only curve with a significant difference between DPPC and POPC. We cannot offer a convincing explanation for this.) For ethanol, the behavior shows almost quasi-long-range order. The reason for this ordering is not clear and further experiments would be needed to study this in detail.

Order parameters

Ordering of the lipid acyl chains is typically characterized by using the order parameter tensor

$$S_{\alpha\beta} = \frac{1}{2}\langle 3\cos\theta_\alpha \cos\theta_\beta - \delta_{\alpha\beta}\rangle, \tag{2}$$

where α, $\beta = x$, y, z, and θ_α is the angle between the αth molecular axis and the bilayer normal (z axis). The order parameter is then computed separately for all carbons along the acyl chain. Since lipid bilayer systems possess symmetry with respect to rotations around the z axis, the relevant order parameter is the diagonal element S_{zz}. To relate S_{zz} to the experimentally relevant deuterium order parameter

$$S_{\text{CD}} = \frac{2}{3}S_{xx} + \frac{1}{3}S_{yy}, \tag{3}$$

we use the symmetry and write $S_{xx} = S_{yy}$, and $S_{xx} + S_{yy} + S_{zz} = 0$. Using these relations we have $S_{\text{CD}} = -S_{zz}/2$. To allow comparison with experimental data, we present our results in terms of $|S_{\text{CD}}|$.

Since our simulations employ a united-atom model, no explicit information about the hydrogen positions is available and they must be reconstructed assuming a perfect tetrahedral arrangement. The results are shown in Fig. 13. Reconstruction of the hydrogen positions means that, for the
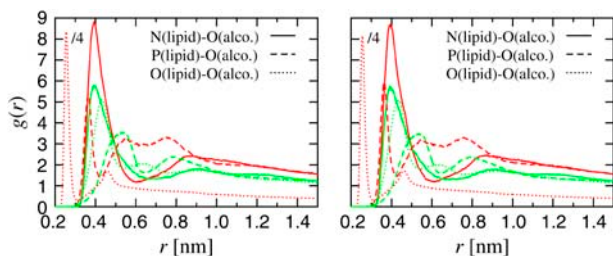

FIGURE 11 Radial-distribution function between the oxygen of alcohol, on the one hand, and the phosphorus and the nitrogen atoms in the head-group as well as the ester oxygens in the lipid chain, on the other hand. The oxygen-oxygen curve has been scaled by a factor of 1/4, i.e., in reality the RDF peaks at a value four times as large as displayed in the figure.
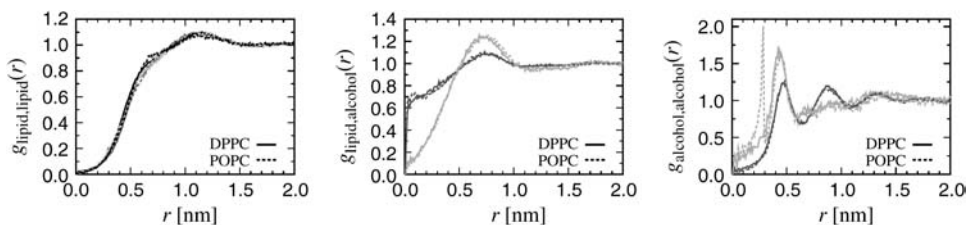
FIGURE 12 Two-dimensional radial-distribution functions of the center-of-mass positions for lipid-lipid (*left*), lipid-alcohol (*center*), and alcohol-alcohol (*right*).

outermost carbon atoms of the chain, no order parameter can be constructed. This also includes positions where a sequence of carbon atoms connected by single bonds ends in a carbon atom having a double bond. It is not a problem to compute the order parameter for a chain of atoms connected by double bonds, but there is a problem connecting such a chain to a chain of atoms connected by single bonds. For this reason, we show the order parameter for both chains of DPPC but for POPC we restrict ourselves to the saturated $sn-1$ chain (see Fig. 1).

The results for the order parameter for all the cases are shown in Fig. 13. We find that for the used concentration both ethanol and methanol slightly enhance the ordering of the lipid acyl chains. Methanol increases ordering close to the glycerol group, whereas the effect of ethanol is strongest below the glycerol group, around the center of the hydrocarbon chains. These results are fully consistent with the mass density profiles in Fig. 6.

As discussed earlier, to our knowledge there is only one other related membrane-alcohol simulation study (12) that also includes experimental data. The authors found through ^{2}H NMR that the addition of ethanol decreases the order parameter, S_{CD}. Since that seems contradictory to our results, we take a more detailed look at the order parameter below.

First, additional insight can be gained by combining the order parameters with the hydrogen-bonding analysis (from Hydrogen Bonding of Alcohol to Lipids, above). This combination allows the computation of the order parameter depending on whether the lipid is involved in hydrogen bonding with an alcohol molecule. The result in Fig. 14 shows

the order parameter for the lipids that are hydrogen-bonded and for those that are not. Fig. 14 shows that binding to an ethanol decreases the order of the chains.

We propose that the order parameter is changed by two separate contributions—a local effect that is due to proximity of alcohol molecules to the lipids and is monotonic with alcohol concentration; and a more global effect that is due to the surface tension of the water-alcohol mixture and is highly nonmonotonic. We are in the regime where the second effect is still increasing with alcohol concentration whereas Feller et al. (12) have a higher concentration (and lower hydration) and are in a different regime, and see a decrease in the order parameter. In our simulations, this is demonstrated by the decrease of the order parameter for the lipids that are bound to ethanols (Fig. 14). Physically, the surface tension is modified by the presence of ethanol.

The experimental and theoretical results of Aratono et al. (43) render support to the above scenario. They studied the effect of ethanol in water solutions in the presence of a water-air interface. They showed that the density of ethanol at the surface is not a monotonous function of the ethanol mole fraction but has a sharp maximum. They observed that at lower mole fractions there were large effects at the surface, whereas at larger mole fractions the effects were smaller and in the opposite direction—as suggested above. They also reported corresponding behavior for other thermodynamic quantities such as the entropy of surface formation.

To test the proposed scenario, we conducted additional simulations following exactly the same simulation protocol as described above, with the only exception that the number
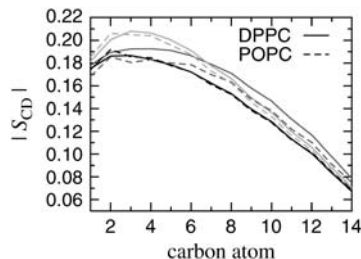

FIGURE 13 Deuterium order parameters, computed from Eq. 3, for DPPC (*solid line*) and POPC (*dashed line*). For DPPC, the average over the two chains is displayed, while for POPC only, the saturated $sn-1$ chain is shown. For numbering of carbon atoms, refer to Fig. 1.
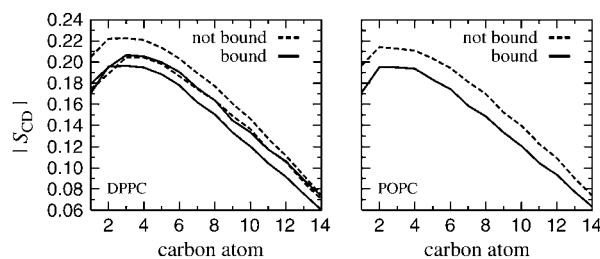

FIGURE 14 Order parameter of DPPC (*left*) and POPC (*right*) in the presence of ethanol. For DPPC, both the $sn-1$ and $sn-2$ chains are shown whereas for POPC only the $sn-1$ chain is depicted. The order parameter has been computed separately for lipids that are bound to at least one alcohol molecule (*solid lines*), and for lipids that are not bound to any alcohol (*dashed lines*).

of alcohol molecules inside the simulation volume was varied between 45 and 450 in steps of 45. As before, we determined the $|S_{CD}|$ order parameter profiles. The results presented in Fig. 15 clearly show that the maximum value of the $|S_{CD}|$ order parameter profile, corresponding to a position close to the glycerol backbone, depends on ethanol concentration in a nonmonotonous fashion. For small ethanol concentrations, the order of the hydrocarbon chains close to the glycerol backbone increases with an increasing ethanol concentration. The order then has a maximum beyond which it decreases monotonously for larger concentrations. On the other hand, the minimum value of $|S_{CD}|$, which describes ordering in the near ends of the acyl chains, simply decreases monotonously for an increasing ethanol concentration. The results in Fig. 15 thus allow us to conclude that the surface tension is indeed modified by the presence of ethanol, and the effect depends on the alcohol concentration.

Fig. 15 settles the issue with regard to the difference between our findings and those of Feller et al. (12). As for other studies, Chin and Goldstein (21) have studied changes in order parameter in natural biomembranes upon addition of ethanol. They found a slight but monotonous reduction in order parameter. However, since their results are for natural biomembranes and describe average ordering in the hydrocarbon chain region (instead of any specific carbon along the chain), a direct comparison to our results is not possible. Nevertheless, the agreement is reasonable, considering the differences in membrane composition and analysis. A more detailed discussion of this issue, i.e., the influence of alcohol concentration, will be presented elsewhere.

In addition to the deuterium order parameter for the acyl chains, it is possible to study the ordering of headgroups in a similar fashion. To do that, we have chosen the angle of the P−N vector with respect to the bilayer interface plane and have computed its distribution. The result is shown in Fig. 16.

FIGURE 16 Distribution of the angle θ between the P−N vector and the bilayer normal for DPPC (*left*) and POPC (*right*).

The P−N vector has a significantly higher tendency of being in the bilayer plane ($\theta = 90°$), than of sticking out of it. The computed distribution is only slightly dependent on the presence of alcohol.

Again, we can obtain additional information for the ethanol systems if the angular distribution is separated into the distributions of lipids that are hydrogen-bonded to an alcohol, and those that are not. The result is shown in Fig. 17. For DPPC the angular distribution is not influenced at all by hydrogen bonding, whereas for POPC the influence is small.

To better explain the results presented in this section, we return to the mass density profiles. We analyzed the positions of the phosphate and the choline groups in the heads of the lipids as well as the lipids' center-of-mass positions, separated into lipids that are hydrogen-bonded or not hydrogen-bonded to an ethanol. The data in Fig. 18 shows that lipid molecules are shifted toward the center of the bilayer by ~0.2 nm if they are bonded to an ethanol molecule. This is in agreement with the reduced order parameter, as that is normally associated with a thinner bilayer. The vertical distance between the choline and the phosphate group remains unchanged, in agreement with the distribution of the P−N angle.

Orientation of the water dipole

Ordering of the water dipole in the vicinity of the bilayer-water interface is described by calculating the time-averaged
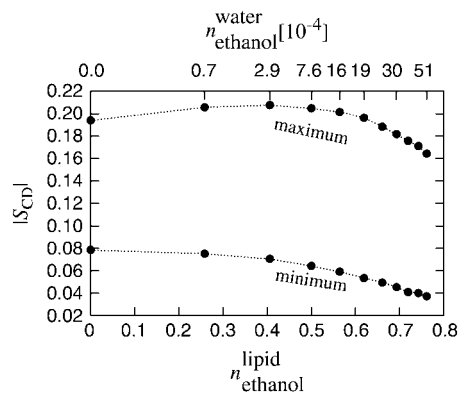

FIGURE 15 Dependence of $|S_{CD}|$ on ethanol concentration. Results shown here are for the maximum and minimum value of the $|S_{CD}|$ order parameter. The number of ethanol molecules ranges from zero to 450. The number of lipid and water molecules used in these simulations was 128 and 9000, respectively. The value n_b^a stands for the molar concentration of component b in phase a.
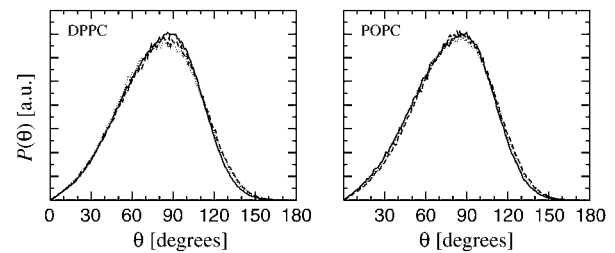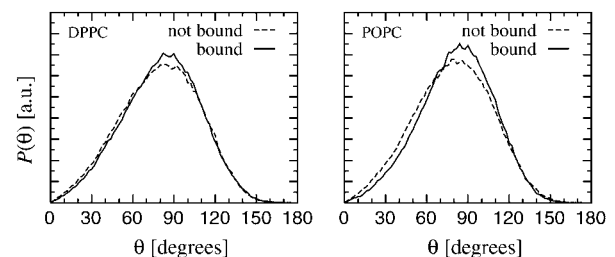

FIGURE 17 Distribution of the angle between the P−N vector and the bilayer normal for DPPC (*left*) and POPC (*right*) in the presence of ethanol. The distribution is separated into lipids that are either hydrogen-bonded or not hydrogen-bonded, respectively, to an ethanol molecule.
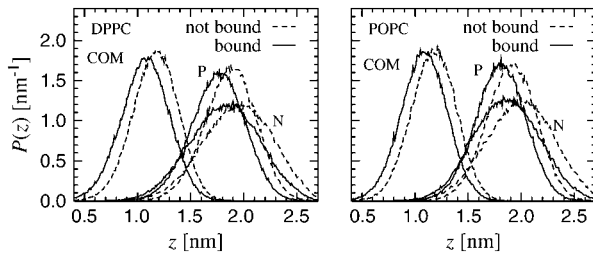
FIGURE 18 Distribution of the position of the phosphate group (P), the choline group (N), and the center-of-mass of the entire lipid (COM); left for DPPC, right for POPC. Results are shown as solid (*dashed*) lines for lipid molecules bound (unbound) to an ethanol molecule. Please note that, in this figure, the colors do not mark the kind of alcohol present.

projection of the water dipole unit vector $\vec{\mu}(z)$ onto the interfacial normal $\vec{n}$,

$$P(z) = \langle \vec{\mu}(z) \cdot \vec{n} \rangle = \langle \cos\theta(z) \rangle, \qquad (4)$$

where z is the z component of the center-of-mass of the water molecule and vector $\vec{n}$ points away from the bilayer center along the z coordinate.

The data for all the studied cases are shown in Fig. 19. For pure bilayers the results are in agreement with previous studies, e.g., Ly and Longo (28). When either methanol or ethanol is added, the water dipole becomes less oriented, i.e., the addition of alcohol slightly reduces the amount of ordering. For pure bilayers, and for bilayers with added methanol, the minimum remains at the same distance, at ~1.8 nm from the bilayer center. For added ethanol, the minimum shifts to a smaller distance, to ~1.6 nm. This is a reflection of the fact that ethanol leads to a slightly larger area per lipid and thus, a thinner bilayer (see System Dimensions, above).

Electrostatic potential

To obtain the electrostatic potential across the bilayer, the average charge density profile was first computed such that the center of the bilayer was separately aligned to $z = 0$ for each simulation frame. Then, the electrostatic potential was determined by integrating the charge density twice with the initial condition $V(z = 0) = 0$.
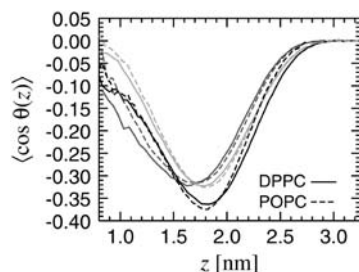
The electrostatic potentials for all studied cases are shown in Fig. 20. For pure DPPC the electrostatic potential was determined to be -589 mV in agreement with previous studies (17,28). For pure POPC, we obtain -507 mV.

The addition of alcohol leads only to small changes in the electrostatic potential. This is what is expected from the results presented so far. The only way in which the membrane potential could be changed significantly would be by rearrangement of the P−N angle of the headgroup, resulting in a change of the dipole moment of the lipid headgroup. No such rearrangement was observed (see Fig. 16).

On a superficial level this may seem to be in contradiction to some previous suggestions that the narcotic effects of alcohols are mainly due to a change of the electrostatic potential. We would like to point out, however, that even though the direct effect of alcohol to the potential is small, this does not exclude secondary effects which may lead to a significant change in the electrostatic potential. We return to this issue in Discussion, below.

Crossing events

Next, we analyze the penetration of alcohol through the membrane. A quick overview can be obtained by plotting the z component of the positions of the alcohol molecules. The result is shown in Fig. 21. The density (in space and time) of alcohol molecules is large in most parts of the diagram such that it is difficult to visually identify individual trajectories.

It is easily seen from Fig. 21 that the density of alcohol molecules is reduced in the center of the bilayer. In addition, the gap in the center of the bilayer is smaller for ethanol than it is for methanol. This is in agreement with the mass density profiles in Mass Density, above. It is also evident that there is a significant number of events where an ethanol molecule is crossing from one leaflet to the other, while no such events are seen for methanol molecules. (Crossing events cannot be inferred from the mass density since these events happen so fast that the resulting mass density of alcohol in the center of the bilayer is negligible.)

In the simulations, it is directly known which atoms form the lipid molecules of the upper leaflet of the bilayer, and
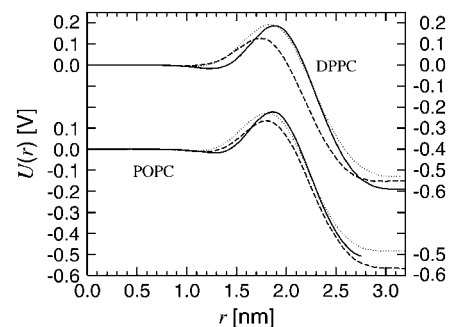

FIGURE 19   Water orientation, as described by the mean cosine of the angle of the water dipole moment with respect to the bilayer normal.

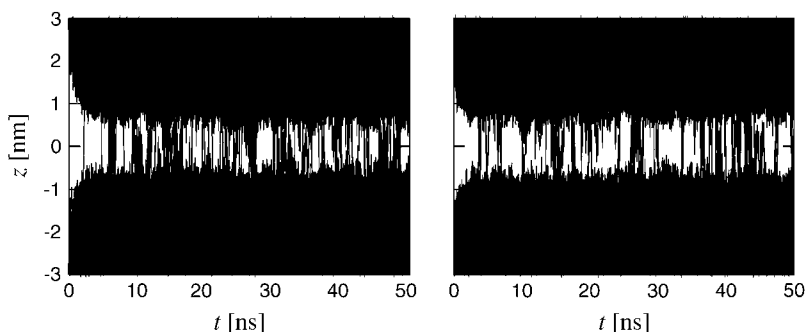FIGURE 20   Electrostatic potential through the bilayer for DPPC (*top*) and POPC (*bottom*).

FIGURE 21 The z-positions of all alcohol molecules as a function of time for DPPC (*left*) and POPC (*right*). Ethanol is able to penetrate into the bilayer (located at $z = 0$) whereas methanol is not (black uniform regions). Crossing events of ethanol are seen while they are completely absent for methanol.

which atoms form the lower leaflet, and which atoms belong to water molecules. The atom nearest to the alcohol molecule then determines in which of the three phases a given alcohol molecule is located at any given moment. In addition, it is also relevant whether an alcohol molecule is hydrogen-bonded to some lipid molecule (see Hydrogen Bonding of Alcohol to Lipids, above).

When all these pieces of information are combined, one arrives at data shown in Fig. 22 in which we depict a few selected ethanol molecules within a DPPC bilayer. It is seen that, while the alcohol is inside the bilayer, it is hydrogen-bonded most of the time, the hydrogen-bond lifetime being ~1 ns (Table 3). However, ethanol molecules can stay inside the bilayer much longer than this. Whenever the hydrogen bond is broken, it can either be reformed shortly afterward, or the alcohol molecule can try to move to some other place. Fig. 22 shows that an alcohol molecule can move to the opposite leaflet of the bilayer but that not all such attempts are successful, i.e., the alcohol molecule may be reflected back.

Using the collected information, each alcohol molecule is at any given moment in one of five different states: water phase, upper leaflet, upper leaflet hydrogen-bonded, lower leaflet, and lower leaflet hydrogen-bonded (we will discuss the methanol-containing systems below). It is of little interest if an alcohol molecule is scratching at the surface of the bilayer—rather, it is important whether the alcohol molecule reaches the part of the leaflet where it can form a hydrogen bond.

This immediately gives functional definitions for different kinetic events that can be used for an analysis. A successful crossing event from the upper to the lower leaflet is, for example, given by the sequence

upper leaflet hydrogen-bonded $\rightarrow$ {upper leaflet}
$\qquad \rightarrow$ {lower leaflet} $\rightarrow$ lower leaflet hydrogen-bonded,

where the brackets mean that this step may also be skipped. Similarly, an unsuccessful crossing from top to bottom would be

upper leaflet hydrogen-bonded $\rightarrow$ {upper leaflet}
$\qquad \rightarrow$ lower leaflet $\rightarrow$ {upper leaflet} $\rightarrow$ upper
$\qquad$ leaflet hydrogen-bonded.

Other criteria are constructed similarly.

Table 4 shows the results of the analysis for crossings of ethanol molecules between the two leaflets. A simple calculation shows that ethanol molecules are able to move from one leaflet to the other on a timescale of 130 ns for DPPC and 180 ns for POPC. The number of unsuccessful crossing attempts outnumbers the number of successful attempts by a factor of 4, thereby demonstrating that the hydrophobic chains of the lipid pose a significant barrier to ethanol not only from the outside of the leaflet but also from the inside. For methanol we did not find any crossing events, implying that the corresponding timescale must be at least of the order of microseconds.

A closer study of the systems containing methanol is hindered by a problem that is not obvious from any of the data presented so far. As Fig. 23 shows, methanol is virtually never really inside the bilayer, i.e., located such that it no longer has direct contact with the bulk water phase—in all of our data for DPPC and POPC with methanol, we found only a single methanol molecule that had actually lost contact with the water phase.
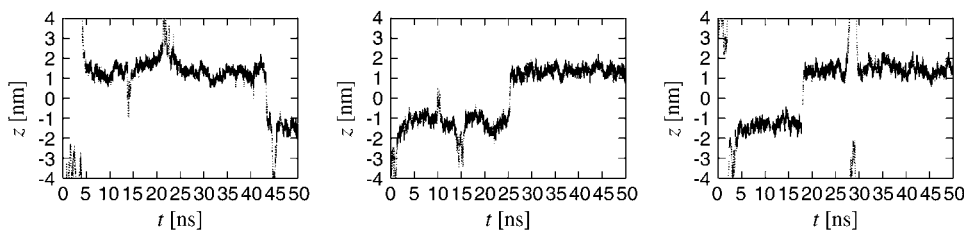

FIGURE 22 The z-component of the center-of-mass position of a few tagged ethanol molecules in a DPPC bilayer system. Each figure depicts the trajectory of a different molecule. We have chosen three out of the 90 molecules to give a demonstration of the possible behavior. Dark solid line means that the a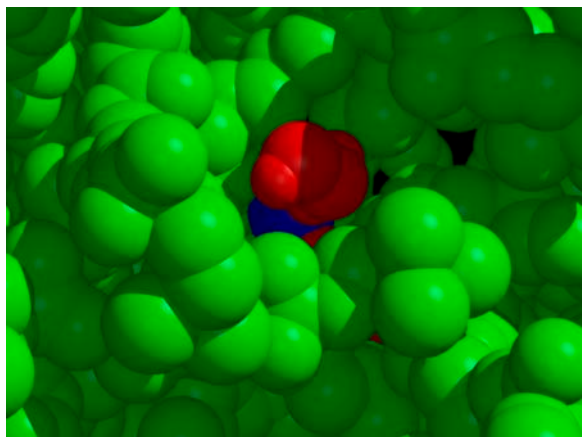lcohol molecule is hydrogen-bonded to a lipid and the dotted line means it is not. As seen, the molecules can cross the bilayer and escape to the water phase.

TABLE 4 Number of successful and unsuccessful crossing events, respectively, within 40 ns of trajectory; in addition, the mean time spent in the crossing process is given
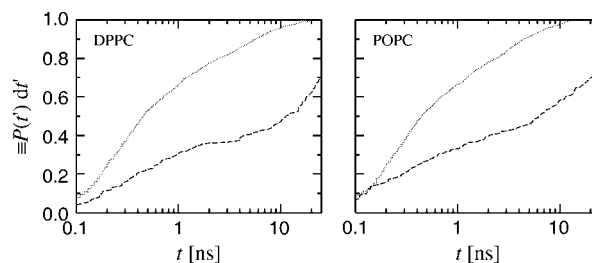
System	Successful		Unsuccessful	
	Number	Time (ps)	Number	Time (ps)
DPPC-ethanol	30	325	123	245
POPC-ethanol	21	375	101	225

FIGURE 24 Distribution $P(t)$ of the time t for which an alcohol molecule stays inside the membrane; left for DPPC, right for POPC. Due to limited statistics, we cannot plot $P(t)$ directly but are limited to the cumulative probability $\int P(t')t'$.

The above observation is also able to explain why no hydrogen bonds are formed between methanol and the lipids: water is an energetically more favorable binding partner for methanol, or, in other words, the surface tension of water is too high for methanol to leave the water phase. The concept of an alcohol being inside the membrane thus does not apply—topologically, methanols are always located outside the membrane. Rather we need to introduce the concept of a methanol being located in a sufficiently deep well. This can be quantified by counting the number of atoms belonging to lipids within a certain distance around some particular methanol molecule. This number will be much larger if the methanol is inside such a well. (We use the criterion that the number of atoms belonging to lipid molecules within 0.6 nm is larger than 50.)

Using that functional definition, we are able to treat ethanol- and methanol-containing systems on a similar footage. Although there are no crossing events for methanol, another interesting question still arises—namely the dynamics of alcohol exchange between the membrane and the water phase. Quantitatively, the interesting quantity is the time t between an alcohol molecule entering the membrane and its subsequent leaving it again. Our results are shown in Fig. 24. Since there are only of the order of 200 (1000) events for ethanol (methanol), the statistics is insufficient to compute the probability distribution $P(t)$. Rather, we present the cumulative probability $\int P(t')dt'$, i.e., the probability that an

alcohol stays inside the membrane no longer than some time t, since this quantity can be computed without binning the data point. ($P(t)$ follows, in principle, by differentiation of the depicted curves.) It is seen from the figure that the dynamics is much faster for methanol than for ethanol. This comes as no surprise since methanol is not really inside the bilayer—it does not need to cross the bilayer interface but only needs to deform it (to create a well).

DISCUSSION

This study is, to the best of our knowledge, the first detailed computational one characterizing the behavior of lipid bilayers (POPC and DPPC) under the influence of methanol and ethanol. The other existing molecular dynamics study of ethanol and POPC (12) concentrated on the comparisons with an NMR study under different hydration conditions and ethanol concentration, and using an *NVT* ensemble in the simulations.

Let us first discuss the area per lipid and bilayer thickness. The increase in the area per lipid is larger for DPPC bilayers (~7% for ethanol and 6% for methanol) as compared to POPC systems (5% for ethanol and 3% for methanol). This compares well with the recent micropipette studies of Ly et al. (10), who used SOPC vesicles under slightly different conditions (20 vol % ethanol at room temperature). They observed 9% increase in the area per lipid and 8% decrease in the thickness of the bilayer. Here, we obtained a decrease of 7%–10% (ethanol and DPPC) and 1%–4% (ethanol POPC) in thickness depending on the definition used (see Eq. 1).

As a purely structural effect, it is clear that the membrane thus becomes more permeable to small molecules due to its increased area per lipid. The differences between DPPC and POPC are most likely due to the slightly longer $sn-2$ chain of POPC and the double bond in it. In addition to the effects captured by the average area per lipid, steric constraints seem to make the POPC bilayer less susceptible to penetration of small solutes.

Furthermore, in a recent study, Chanturiya et al. (44) proposed that the penetration of alcohols inside the bilayer and their binding at it, as well as the resulting decrease in bending

FIGURE 23 View from the top onto part of a POPC bilayer with methanol. (The lipids are colored *green*, methanol is colored *blue*, and a few selected water molecules are shown in *red*.) It is easily seen than the methanol is located in a cavity together with a few water molecules.

rigidity, is a feasible pathway for promoting fusion of cells. Although it is not possible to probe this directly by current computer resources, our observations support the possibility of such a mechanism.

It has been suggested that the preferred location of ethanol close to the membrane dehydrates it (6,42,45). This should show in the water dipole orientation data (see Fig. 19). The relatively small changes in it, and in the electrostatic potential across the membrane, suggest that indirect effects, such as receptor blocking, may be more important in producing changes in these quantities.

Short-chain alcohols have an amphiphilic character and it has been known for a long time that addition of each new CH_2 group—adding a CH_2 group on methanol gives ethanol, and so on—has a strong effect on the interactions with membranes. This is indicated by the well-known Traube's rule (46,47), which states that the addition of a new CH_2 group leads to a decrease in surface tension. In other words, short-chain alcohols have a strong effect on membrane properties and the effect depends on both the length of the hydrophobic part of the alcohol and on concentration. This has also been observed in recent experiments (10,11).

Our data for methanol and ethanol supports these conclusions. Methanol does not penetrate through the lipid chain region, easily understood by the hydrophobic nature of the lipid chains, which are repelling methanol because it is more polar than ethanol. As a second effect, methanol rarely reaches the chain region as each methanol molecule moves together with a small cluster of water molecules when it is trying to enter the membrane. This means that, on one hand, methanol is pulled back into the water phase by this, and, on the other hand, not a single small methanol molecule but a significantly larger dressed particle, or a small cluster, would need to penetrate the membrane.

The analysis of crossing events, i.e., how often the molecules travel through the membrane, showed that ethanol is able to penetrate the membrane easily, whereas, for methanol, not a single crossing event was observed. This confirms the interpretation given above. It is difficult to compare these results directly with experiments, but the possibility of such crossing events has been proposed on the basis of NMR studies (42). The results presented here are, to our knowledge, the first detailed analysis of crossing events. Further experiments would be needed to better characterize the situation as the system here is a simple model system and the relevance of these results to biological systems, in particular yeasts, needs to be better studied. The only such a study we were able to find uses NMR and *Zymomonas mobilis* (48), but direct comparison is not possible due to the different experimental setup.

Figs. 13 and 14 show a surprising finding, namely, that the overall order parameter increases slightly (in comparison with the pure system) when alcohol is added in the system. This seems to be in contradiction with recent experiments and simulations (12). That is not the case, however. Let us first list the observations. First of all, the ethanol concentration and hydration level here is lower than in the study of Feller et al. (12), and second, Fig. 14 shows that the order parameter decreases for the lipids that are bound to ethanol molecules, whereas it is higher for the lipids that remain unbound. As less than half of the lipids are bound (Table 3), the overall effect is a slight increase in the total order parameter. Thus, we propose that the overall effect of ethanol depends on concentration and hydration: we are in the regime in which the overall order parameter still increases but as Feller et al. (12) have a higher concentration (and lower hydration), they are in a different regime and see a decrease in the order parameter—in our simulations this is demonstrated by the decrease of the order parameter for the lipids that are bound to ethanols (Fig. 14).

The above scenario is supported by the experimental and theoretical results of Aratono et al. (43), who studied the effect of ethanol in water solutions in the presence of a water-air interface. In particular, they showed that the density of ethanol at the surface is not a monotonous function of the ethanol mole fraction but has a sharp maximum. They observed that at lower mole fractions there were large effects at the surface, whereas at larger mole fractions the effects were smaller and in the opposite direction. Corresponding behavior was also reported for other thermodynamic quantities such as the entropy of surface formation.

To confirm this nonmonotonic behavior and to resolve the apparent contradiction between our results and those of Feller et al. (12), we run additional simulations in which the ethanol concentration was varied over a wide range. The results (see Fig. 15) showed that the ordering of hydrocarbon chains close to the glycerol backbone, where ethanol likes to reside, depends on ethanol concentration. For small concentrations the ordering increases, while for larger concentrations of ethanol the ordering decreases monotonously. As the studies of Feller et al. (12) were conducted at a larger ethanol concentration than in this work, this explains their observation that the ordering of hydrocarbon chains under the influence of ethanol was reduced compared to a pure bilayer. These results therefore support the scenario that alcohols affect the surface tension at the lipid-water interface (43), and hence their influence on membrane properties depends on alcohol concentration in an intricate fashion.

Summarizing, the results of the present simulation study are in line with experiments in cases where a comparison is possible. We have found the area per lipid to increase due to alcohols, as observed in experiments by Ly et al. (10). Ethanol prefers to be accommodated in the vicinity of the lipid headgroup region, in agreement with experimental data (42). The lifetime of hydrogen bonding between ethanol and lipid headgroups is also consistent with the data of Holte and Gawrisch (42). As for ordering of hydrocarbon chains, we have shown that the effect due to an increasing ethanol concentration is nonmonotonous, in agreement with results given and ideas suggested by Aratono et al. (43), and also in line with

other studies showing a decrease of chain order (see (12,21)). As for partitioning of alcohols, its alcohol concentration-dependence, and other concentration-dependent features, we shall discuss elsewhere.

In the Introduction we briefly discussed general anesthesia and membrane-protein interactions induced by the addition of anesthetics, such as small alcohols. This was observed in a recent experiment (49) where the potassium channel KcsA was observed to dissociate due to the changes in lateral membrane pressure induced by small alcohols. Here, we have characterized simple membrane-alcohol systems. The detailed characterization presented here is essential for extensive simulational studies of membrane-protein-anesthetic systems. From our results it is obvious that the changes in pure membranes are subtle, but the effects of those changes to, e.g., embedded proteins may be significant (3–5,15,49). This is also supported by recent experiments using enflurane and DPPC (50). Similar conclusions have been drawn by Tu et al. (38) for the interaction of halothane with bilayers. As pointed out by Hauet et al. (50), there are various intriguing questions regarding small molecules and anesthesia. These questions are related to interactions between membranes and small molecules, and computer simulations give a direct access to study them.

REFERENCES

1. Cantor, R. S. 2003. Receptor desensitization by neurotransmitters in membranes: are neurotransmitters the endogenous anesthetics? *Biochemistry.* 42:11891–11897.

2. Mazzeo, A. R., J. Nandi, and R. A. Levine. 1988. Effects of ethanol on parietal cell membrane phospholipids and proton pump function. *Am. J. Physiol.* 254:G57–G64.

3. Cantor, R. 1997. The lateral pressure profile in membranes: a physical mechanism of general anesthesia. *Biophys. J.* 36:2339–2344.

4. Eckenhoff, R. G. 2001. Promiscuous ligands and attractive cavities. How do the inhaled anesthetics work? *Mol. Interv.* 1:258–268.

5. Tang, P., and Y. Xu. 2002. Large-scale molecular dynamics simulations of general anesthetic effects on the ion channel in the fully hydrated membrane: the implication of molecular mechanisms of general anesthesia. *Proc. Natl. Acad. Sci. USA.* 99:16035–16040.

6. Klemm, W. R. 1998. Biological water and its role in the effects of alcohol. *Alcohol.* 15:249–267.

7. Bisson, L. F., and D. E. Block. 2002. Ethanol tolerance in *Saccharomyces. In* Biodiversity and Biotechnology of Wine Yeasts. M. Ciani, editor. Research Signpost, Kerala. 85–98.

8. da Silveira, M. G., E. A. Golovina, F. A. Hoekstra, F. M. Rombouts, and T. Abee. 2003. Membrane fluidity adjustments in ethanol-stressed *Oenococcus oeni* cells. *Appl. Environ. Microbiol.* 69:5826–5832.

9. Cramer, A. C., S. Vlassides, and D. E. Block. 2002. Kinetic model for nitrogen-limited wine fermentations. *Biotechnol. Bioeng.* 77:49–60.

10. Ly, H. V., D. E. Block, and M. L. Longo. 2002. Interfacial tension effect on lipid bilayer rigidity, stability, and area/molecule: a micropipette aspiration approach. *Langmuir.* 18:8988–8995.

11. Ly, H. V., and M. L. Longo. 2004. The influence of short-chain alcohols on interfacial tension, mechanical properties, area/molecule, and permeability of fluid lipid bilayers. *Biophys. J.* 87:1013–1033.

12. Feller, S. E., C. A. Brown, D. T. Nizza, and K. Gawrisch. 2002. Nuclear Overhauser enhancement spectroscopy cross-relaxation rates and ethanol distribution across membranes. *Biophys. J.* 82:1396–1404.

13. Lee, B. W., R. Faller, A. K. Sum, I. Vattulainen, M. Patra, and M. Karttunen. 2004. Structural effects of small molecules on phospholipid bilayers investigated by molecular simulations. *Fluid Phase Equil.* 225:63–68.

14. Bemporad, D., J. W. Essex, and C. Luttmann. 2004. Permeation of small molecules through a lipid bilayer: a computer simulation study. *J. Phys. Chem. B.* 108:4875–4884.

15. Koubi, L., M. Tarek, S. Bandyopadhyay, M. L. Klein, and D. Scharf. 2001. Membrane structural perturbations caused by anesthetics and nonimmobilizers: a molecular dynamics investigation. *Biophys. J.* 81:3339–3345.

16. Koubi, L., M. Tarek, M. L. Klein, and D. Scharf. 2000. Distribution of halothane in a dipalmitoylphosphatidylcholine bilayer from molecular dynamics calculations. *Biophys. J.* 78:800–811.

17. Tieleman, D. P., and H. J. C. Berendsen. 1996. Molecular dynamics simulations of a fully hydrated dipalmitoylphosphatidylcholine bilayer with different macroscopic boundary conditions and parameters. *J. Chem. Phys.* 105:4871–4880.

18. Patra, M., M. Karttunen, M. T. Hyvönen, E. Falck, and I. Vattulainen. 2004. Lipid bilayers driven to a wrong lane in molecular dynamics simulations by subtle changes in long-range electrostatic interactions. *J. Phys. Chem. B.* 108:4485–4494.

19. Falck, E., M. Patra, M. Karttunen, M. T. Hyvönen, and I. Vattulainen. 2004. Lessons of slicing membranes: interplay of packing, free area, and lateral diffusion in phospholipid/cholesterol bilayers. *Biophys. J.* 87:1076–1091.

20. Tieleman, D., M. Sansom, and H. Berendsen. 1999. Alamethicin helices in a bilayer and in solution: molecular dynamics simulations. *Biophys. J.* 76:40–49.

21. Chin, J. H., and D. B. Goldstein. 1977. Drug tolerance in biomembranes: a spin label study of the effects of ethanol. *Science.* 196:684–685.

22. Berger, O., O. Edholm, and F. Jahnig. 1997. Molecular dynamics simulations of a fluid bilayer of dipalmitoylphosphatidylcholine at full hydration, constant pressure, and constant temperature. *Biophys. J.* 72:2002–2013.

23. Lindahl, E., B. Hess, and D. van der Spoel. 2001. GROMACS 3.0: a package for molecular simulation and trajectory analysis. *J. Mol. Mod.* 7:306–317.

24. Berendsen, H. J. C., J. P. M. Postma, W. F. van Gunsteren, and J. Hermans. 1981. Interaction models for water in relation to protein hydration. *In* Intermolecular Forces. B. Pullman, editor. Reidel, Dordrecht. 331–342.

25. Berendsen, H. J. C., J. P. M. Postma, W. F. van Gunsteren, A. DiNola, and J. R. Haak. 1984. Molecular dynamics with coupling to an external bath. *J. Chem. Phys.* 81:3684–3690.

26. Hess, B., H. Bekker, H. J. C. Berendsen, and J. G. E. M. Fraaije. 1997. LINCS: a linear constraint solver for molecular simulations. *J. Comput. Chem.* 18:1463–1472.

27. Kessel, A., D. Tieleman, and N. Ben-Tal. 2004. Implicit solvent model estimates of the stability of model structures of the alamethicin channel. *Eur. Biophys. J.* 33:16–28.

28. Patra, M., M. Karttunen, M. Hyvönen, E. Falck, P. Lindqvist, and I. Vattulainen. 2003. Molecular dynamics simulations of lipid bilayers:

major artifacts due to truncating electrostatic interactions. *Biophys. J.* 84:3636–3645.

29. Essman, U., L. Perela, M. L. Berkowitz, H. L. T. Darden, and L. G. Pedersen. 1995. A smooth particle-mesh Ewald method. *J. Chem. Phys.* 103:8577–8592.

30. Chiu, S. W., E. Jakobsson, S. Subramanian, and H. L. Scott. 1999. Combined Monte Carlo and molecular dynamics simulation of fully hydrated dioleyl and palmitoyl-oleyl phosphatidylcholine lipid bilayers. *Biophys. J.* 77:2462–2469.

31. Pasenkiewicz-Gierula, M., T. Róg, J. Grochowski, P. Serda, R. Czarnecki, T. Librowski, and S. Lochyński. 2003. Effects of carane derivative local anesthetic on a phospholipid bilayer studied by molecular dynamics simulation. *Biophys. J.* 85:1248–1258.

32. Pabst, G., M. Rappolt, H. Amenitsch, S. Bernstorff, and P. Laggner. 2000a. X-ray kinematography of temperature-jump relaxation probes the elastic properties of fluid bilayers. *Langmuir.* 16:8994–9001.

33. Pabst, G., M. Rappolt, H. Amenitsch, and P. Laggner. 2000b. Structural information from multilamellar liposomes at full hydration: full *q*-range fitting with high quality x-ray data. *Phys. Rev. E.* 62:4000–4009.

34. Armen, R. S., O. D. Uitto, and S. E. Feller. 1998. Phospholipid component volumes: determination and application to bilayer structure calculations. *Biophys. J.* 75:734–744.

35. Vogel, M., C. Münster, W. Fenzl, and T. Salditt. 2000. Thermal unbinding of highly oriented phospholipid membranes. *Phys. Rev. Lett.* 84:390–393.

36. Gullingsrud, J., and K. Schulten. 2004. Lipid bilayer pressure profiles and mechanosensitive channel gating. *Biophys. J.* 86:3496–3509.

37. Nagle, J. F., and S. Tristram-Nagle. 2000. Structure of lipid bilayers. *Biochim. Biophys. Acta.* 1469:159–195.

38. Tu, K., M. Tarek, M. L. Klein, and D. Scharf. 1998. Effects of anesthetics on the structure of a phospholipid bilayer: molecular dynamics investigation of halothane in the hydrated liquid crystal phase of dipalmitoylphosphatidylcholine. *Biophys. J.* 75:2123–2134.

39. Löbbcke, L., and G. Cevc. 1995. Effects of short-chain alcohols on the phase behavior and interdigitation of phosphatidylcholine bilayer membranes. *Biochim. Biophys. Acta.* 1237:59–69.

40. Nagle, J. F., R. Zhang, S. Tristram-Nagle, W. Sun, H. I. Petrache, and R. M. Suter. 1996. X-ray structure determination of fully hydrated L_α phase dipalmitoylphosphatidylcholine bilayers. *Biophys. J.* 70:1419–1431.

41. Adachi, T. 2000. A new method for determining the phase in the x-ray diffraction structure analysis of phosphatidylcholine/alcohol. *Chem. Phys. Lipids.* 17:93–97.

42. Holte, L. L., and K. Gawrisch. 1997. Determining ethanol distribution in phospholipid multilayers with MAS-NOESY spectra. *Biochemistry.* 36:4669–4674.

43. Aratono, M., T. Toyomasu, M. Villeneuve, Y. Uchizono, T. Takiue, K. Motomoura, and N. Ikeda. 1997. Thermodynamic study on the surface formation of the mixture of water and ethanol. *J. Colloid Interface Sci.* 191:146–153.

44. Chanturiya, A., E. Leikina, J. Zimmerberg, and L. V. Chernomordik. 1999. Short-chain alcohols promote an early stage of membrane hemifusion. *Biophys. J.* 77:2035–2045.

45. Klemm, W. R. 1990. Dehydration. *Alcohol.* 7:49–59.

46. Adamson, A. W., and A. P. Gast. 1997. Physical Chemistry of Surfaces, 6th Ed. Wiley-Interscience, New York.

47. Traube, I. 1891. Ueber die Capillaritätsconstanten organischer Stoffe in wässerigen Lösungen. (About the capillarity constants of organic materials in watery solutions.) *Justus Liebigs Ann. Chem.* 265:27–55.

48. Schobert, S. M., B. E. Chapman, P. W. Kuchel, R. M. Wittig, J. Grotendorst, P. Jansen, and A. A. de Graaf. 1996. Ethanol transport in *Zymomonas mobilis* measured by using in vivo nuclear magnetic resonance spin transfer. *J. Bacteriol.* 178:1756–1761.

49. van den Brink-van der Laan, E., V. Chupin, J. A. Killian, and B. de Kruijff. 2004. Small alcohols destabilize the KcsA tetramer via their effect on the membrane lateral pressure. *Biochemistry.* 43:5937–5942.

50. Hauet, N., F. Artzner, F. Boucer, C. Grabielle-Madelmont, I. Cloutier, G. Keller, P. Leiseur, D. Durand, and M. Paternostre. 2003. Interaction between artificial membrane and enflurane, a general volatile anesthetic: DPPC-enflurane interaction. *Biophys. J.* 84:3123–3137.